Discussion of thermodynamic features within the PNJL model[*]

Jin-Li Zhang(张金利)[1]   Cheng-Ming Li(李程明)[1]   Hong-Shi Zong(宗红石)[1,2,3;1]

[1] Department of Physics, Nanjing University, Nanjing 210093, China
[2] Joint Center for Particle, Nuclear Physics and Cosmology, Nanjing 210093, China
[3] State Key Laboratory of Theoretical Physics, Institute of Theoretical Physics, CAS, Beijing 100190, China

Abstract: We discuss some thermodynamical features of a QCD system within the two-flavor Polyakov loop extended Nambu–Jona-Lasinio (PNJL) model. Several thermodynamical quantities of interest (pressure, energy density, specific heat, speed of sound, etc.) are investigated and discussed in detail with two different forms of Polyakov loop potential. The effective coupling strength G incorporating a quark feedback (quark condensate) through operator product expansion is also discussed, as well as the relationship between color deconfinement and chiral phase crossover. We find that some thermodynamical quantities have quite different behavior for different Polyakov loop potentials. By changing the characteristic temperature T_0 of the pure Yang-Mills field, we find that when T_0 becomes small, color deconfinement might happen earlier than chiral phase crossover, while their relationship can be determined via some thermodynamical quantities. Furthermore, the behavior of the thermodynamical quantities is quite different in the two different forms of Polyakov loop potential studied. Especially, one of the potentials, specific heat, has two peaks, which correspond to color deconfinement and chiral phase crossover respectively. This interesting phenomenon may shed some light on whether the inflection points of the chiral condensate and deconfinement transitions happen at the same temperature or not for lattice QCD and experimental studies.

Keywords: deconfinement, specific heat, transition temperature

PACS: 12.38.Mh, 12.39.-x, 25.75.Nq   **DOI:** 10.1088/1674-1137/42/12/123105

1   Introduction

Color confinement and dynamical chiral symmetry breaking (DCSB) are two of the most fascinating features of QCD. Many people have devoted themselves to the study of the two topics, and these studies help us to have a better understanding of strongly interacting matter. Both features are associated with QCD Lagrangian global symmetries. However, the relationship of DCSB and color confinement is still an open issue. The chiral phase transition is related to chiral symmetry restoration in the zero current quark mass limit (i.e. $m_q \rightarrow 0$). When heavy-quark masses become infinite (i.e. $m_q \rightarrow \infty$) in the quenched limit, QCD becomes a pure gauge $SU(3)$ theory, which has center symmetry in the vacuum, and the usual order parameter is a Polyakov loop. The question is then the nature of these phase transitions for light quark masses between the two limits [1]. At intermediate masses both transitions develop a fascinating interplay, but this is not yet understood clearly. To explore this issue, non-perturbative methods can be used, such as lattice gauge theory and functional methods.

It is accepted that the dominant ground state nature of QCD can be represented by non-perturbative spontaneous breaking and/or restoring of some of the global symmetries of the QCD Lagrangian [2]. However, it is not easy to describe QCD in the non-perturbative region. Lattice QCD can calculate the transition temperature, equation of state (EoS) of QCD matter and other things from first principles when the quark chemical potential is zero and small. At large chemical potential, due to the sign problem, it is hard to calculate. In this case, many effective models have been proposed in order to explore the non-perturbative region. The Nambu–Jona-Lasinio (NJL) model is a very popular effective model [3, 4]. Of primary significance is the fact that the model Lagrange density is built such that the symmetries of QCD observed in nature are part and parcel of it. One of the most important of these is the chiral symmetry. However, the NJL model ignores gluon dynamics, the interactions among quarks being described by effective four-fermion contact interactions. On account of the absence of gluons, one of the main characteristics of low-energy QCD at small temperature and chem-

ical potential, namely, confinement, is missing in this model [5]. A more hopeful model is the Polyakov loop extended Nambu–Jona-Lasinio (PNJL) model, a combination of Polyakov loop dynamics and the NJL model, combining confinement and spontaneous chiral symmetry breaking. The PNJL model assumes that a homogeneous Euclidean temporal background gluon field [2] combines with quarks by means of the covariant derivative of QCD. This combination leads to the interaction effect of the Polyakov loop and chiral condensate. Furthermore, it is very easy to calculate and has been proved to be a powerful model which can compare several thermodynamical quantities [1, 6, 7] with lattice QCD, because the model can calculate them as well. The PNJL model has therefore been widely used [2, 5, 8–18] and has been very successful in describing many thermodynamic properties of QCD.

Experimentally, at CERN and Brookhaven, recent heavy ion collision experiments have attempted to probe the nature of quark-gluon plasma. Obviously, a theoretical understanding of the fundamental physics is most important. To give first-principles results for thermodynamic quantities, a great many lattice QCD calculations were performed e.g. speed of sound (ν_s) and EoS. For strong interaction physics, one of the primary challenges is to determine the EoS of the dense matter which comes into being after nuclear collisions at ultrarelativistic energies. The EoS offers an elementary characterization of finite temperature QCD. Especially, there are recent results on hydrodynamic flow, jet quenching and charmonium production from the Relativistic Heavy Ion Collider (RHIC) [19–21]. Explanation of the results, on one hand, depend on a precise determination of pressure (P) and energy density (ϵ) as a function of temperature. On the other hand, we should have a deep understanding of the chiral phase transition and deconfinement [22]. The EoS is the functional relationship between ϵ and P in the hypothesis of local thermal equilibrium [23]. P and ϵ are associated with each other by $\nu_s = \left(\frac{\partial P}{\partial \epsilon}\right)_{\text{isentropic}}$. In hydrodynamical evolution of the matter produced in heavy-ion collisions, ν_s plays a key role.

From lattice QCD with temporary extent $N_\tau = 4,6$ and $N_\tau = 8$ [22], we get the most plentiful calculation results of the EoS carried out with $p4$ and asqtad staggered fermion formulations [24, 25]. Lattice QCD calculations will offer pivotal guidance in phenomenological explanation of experimental measurements in quantifying the variation of EoS with transport coefficients and the heavy quark potential as a function of temperature. In this paper we have calculated pressure, entropy density, energy density, interaction measure, specific heat and speed of sound. We have plotted their dependence on temperature and compared the results with different T_0, where T_0 is the first-order deconfinement phase transition point of pure gauge theory.

This paper is organized as follows. In Section 2, we give a brief introduction to the two versions of the PNJL model and our results with parameter $T_0 = 170$ MeV. In Section 3, calculations of the QCD thermodynamic quantities in the framework of the PNJL model are plotted. In Section 4, we calculate the T_0 dependence of QCD thermodynamic quantities, and plot their behaviors for four different values of T_0. A brief summary and discussion are given in Section 5.

2   The PNJL model

The Lagrangian density of the two-flavor (N_f=2) and three-color (N_c=3) PNJL model is given by

$$\mathcal{L}_{\text{PNJL}} = \bar{\psi}(i\gamma^\mu D_\mu - \hat{m}_q)\psi + G\left(\left(\bar{\psi}\psi\right)^2 + \left(\bar{\psi}i\gamma_5\tau\psi\right)^2\right)$$
$$- \mathcal{U}(\Phi(A),\bar{\Phi}(A),T), \tag{1}$$

where the quark field is $\psi = (\psi_u, \psi_d)^T$ and $m_q = \text{diag}(m_u, m_d)$ is the current quark mass matrix with $m_u = m_d = m_q$. G is the effective coupling strength of the four-point interaction of the quark fields. $\mathcal{U}(\Phi(A),\bar{\Phi}(A),T)$ is the Polyakov potential, with $\Phi(A)$ and $\bar{\Phi}(A)$ the Polyakov loop operators. The covariant derivative is determined as

$$D_\mu = \partial_\mu - iA^\mu,$$
$$A^\mu = \delta_{\mu 0}A^0, \tag{2}$$

where the strong coupling strength g has been assimilated in the $SU(3)$ gauge field $A^\mu(x) = g\mathcal{A}_a^\mu(x)\frac{\lambda_a}{2}$, where λ_a are the Gell-Mann matrices.

The constant field ϕ, with matrix values related to the (traced) Polyakov loop operator, is defined as:

$$\phi(\vec{x}) = \frac{1}{N_c}\langle tr_c\mathcal{P}(\vec{x})\rangle. \tag{3}$$

The Polyakov-loop operator $tr_c\mathcal{P}(\vec{x})$ in the fundamental representation of $SU(N_c)$ gauge group contains the temporal vector field A_0,

$$\mathcal{P}(\vec{x}) = P\exp\left(i\int_0^\beta A_0(\vec{x},\tau)\mathrm{d}\tau\right), \tag{4}$$

where $\beta = \frac{1}{T}$ is the inverse temperature, and P denotes the path ordering [26, 27]. In this model, the Polyakov loop serves as a classical variable, thus details of the implementation in Eq. (4) are not significant for our work. The expectation value of Eq. (3) can act as an order parameter of the confinement/deconfinement transition. At low temperatures it is zero and represents the confined phase, and at high temperatures, it becomes non-zero in the deconfined phase. We use the susceptibility of the Polyakov-loop ϕ to determine the transition point [27].

With the quark propagator $S(p)$, the gap equation is

$$M = m_q + 2G\int \frac{\mathrm{d}^4 p}{(2\pi)^4}\text{Tr}[S(p)], \tag{5}$$

where the trace is taken in color, flavor and Dirac space. From Eq. (1) we can see that the interaction between quarks and gluons has been simplified into a local point like four-fermion interactions. This makes the theory divergent, so it is necessity to introduce a cutoff. We will use a three-dimensional cutoff Λ in this paper. One obtains $M = 314$ MeV from Eq. (5) in the PNJL model. The thermodynamic potential per unit volume can be determined in the mean field approximation [28] as:

$$\Omega = \mathcal{U}\left(\phi,\bar{\phi},T\right)+G\left\langle\bar{\psi}\psi\right\rangle^2-6N_f\int^{\Lambda}\frac{\mathrm{d}^3p}{(2\pi)^3}E_p$$
$$-2N_fT\int\frac{\mathrm{d}^3p}{(2\pi)^3}\left[\log(f_1)+\log(f_2)\right], \qquad (6)$$

where

$$f_1=1+\mathrm{e}^{-\frac{3(E_P-\mu)}{T}}+3\left(\phi+\bar{\phi}\mathrm{e}^{-\frac{E_P-\mu}{T}}\right)\mathrm{e}^{-\frac{E_P-\mu}{T}},$$
$$f_2=1+\mathrm{e}^{-\frac{3(E_P+\mu)}{T}}+3\left(\bar{\phi}+\phi\mathrm{e}^{-\frac{E_P+\mu}{T}}\right)\mathrm{e}^{-\frac{E_P+\mu}{T}}, \quad (7)$$

where Λ is the three-momentum cutoff, and the quark quasi-particle energy is defined as $E_p=\sqrt{\vec{p}^2+M^2}$. The reason why the cutoff is only applied to the third term (zero-point energy) is that the fourth term has a natural cutoff given by temperature.

When Ω is known in the PNJL model, we can get the numerical values of $\bar{\psi}\psi$, ϕ and $\bar{\phi}$ for a given (T, μ) using the set formulas as follows in a self-consistent way:

$$\frac{\partial\Omega}{\partial\left\langle\bar{\psi}\psi\right\rangle}=\frac{\partial\Omega}{\partial\phi}=\frac{\partial\Omega}{\partial\bar{\phi}}=0, \qquad (8)$$

at vanishing chemical potential, $\bar{\phi}=\phi$.

Pure gauge lattice QCD thermodynamics is produced again for T up to about double the deconfinement transition temperature determined by $\mathcal{U}\left(\Phi,\bar{\Phi},T\right)$. Transverse gluons begin to dominate at much higher temperature, and in this region we cannot apply the PNJL model [29]. The center symmetry of the pure Yang-Mills theory has been preserved in the Polyakov loop potential [30, 31]. However, there are several explicit forms of Polyakov loop potential [2]. We will use two forms for comparison in the next subsection.

2.1 Polyakov loop potentials

In the pure gauge limit (i.e. $m_q \to \infty$), stimulated by the underlying symmetries of QCD, the functional form of the Polyakov-loop potential can be obtained. Due to the lack of dynamical quarks, the Polyakov loop potential is constructed in such a way that the QCD pure gauge lattice data, thermodynamical quantities (P, ϵ and ν_s), and the critical temperature of deconfinement for heavy (non-dynamical) quarks can be reproduced. The deconfinement temperature $T_0 = 270$ MeV in the pure gauge sector is consistent with lattice QCD results [2, 28, 32, 33]. The original form of the Polyakov loop is

defined as (Potential I):

$$\frac{\mathcal{U}_{\mathrm{poly}}}{T^4} = -\frac{b_2}{2}\left(\bar{\phi}\phi\right)+\frac{b_4}{4}\left(\bar{\phi}\phi\right)^2-\frac{b_3}{6}\left(\bar{\phi}^3+\phi^3\right), \qquad (9)$$

where the expansion coefficients are determined by reproducing thermodynamic lattice QCD results for the pure Yang-Mills sector [28, 34]. The temperature-dependent coefficients are

$$b_2(T)=a_0+a_1\left(\frac{T_0}{T}\right)+a_2\left(\frac{T_0}{T}\right)^2+a_3\left(\frac{T_0}{T}\right)^3. \qquad (10)$$

The corresponding parameters for Potential I are given in Table 1.

Table 1.   Parameter set used for Potential I.

a_0	a_1	a_2	a_3	b_3	b_4
6.75	-1.95	2.625	-7.44	0.75	7.5

An updated Polyakov loop potential ansatz [29] is (Potential II):

$$\frac{\mathcal{U}_{\mathrm{log}}}{T^4} = -\frac{a(T)}{2}\bar{\phi}\phi+b(T)$$
$$\times\log\left(1-6\bar{\phi}\phi+4\left(\bar{\phi}^3+\phi^3\right)-3\left(\bar{\phi}\phi\right)^2\right), \quad (11)$$

with the temperature dependent coefficients

$$a(T)=a_0+a_1\left(\frac{T_0}{T}\right)+a_2\left(\frac{T_0}{T}\right)^2, \qquad (12)$$

and

$$b(T)=b_3\left(\frac{T_0}{T}\right)^3, \qquad (13)$$

Here, what is different from the upper polynomial Polyakov loop potential ansatz is that the logarithms restrict $\bar{\phi}$ and ϕ to smaller than 1. Based on pure gauge lattice data, the parameters of Eq. (11) are given by Ref. [29] and are shown in Table 2.

Table 2.   Parameter set used for Potential II.

a_0	a_1	a_2	b_3
3.51	-2.47	15.2	-1.75

The parameters of the two versions are fitted to reproduce the Polyakov loop expected value and EoS equivalently well. The fit of $T_0 = 270$ MeV was constrained by requiring that the Stefan-Boltzmann limit is achieved at $T \to \infty$ and by enforcing a first-order phase transition at $T_0 = 270$ MeV in the model. The running coupling α changes with the variation of fermionic contributions when dynamical quarks exist. The perturbation theory can estimate the size of this effect, see e.g. Refs. [2, 5, 29, 35]. This will make the expansion coefficients have an N_f dependent correction in the Polyakov loop potential. At zero temperature, Λ_{QCD} will have an N_f

dependent decrease, which at finite temperature will convert into an N_f dependent decrease of the critical temperature T_0. For details see Ref. [36].

Table 3 shows the values of T_0 for different N_f. The value for 2+1 flavors is estimated with a massive strange quark mass of $m_s = 150$ MeV. In Ref. [36], they work with $N_f = 2$ and use a critical temperature $T_0(2) = 192$ MeV. These parameters are for massless quarks. When we consider that quarks have mass, the temperature will be lower. We therefore use $T_0 = 170$ MeV as an example. In Section 4 the T_0-dependence of phase structure, heat capacity, entropy density and speed of sound are investigated for Potential I and Potential II in detail.

Table 3. The critical temperature T_0 for N_f massless flavors.

N_f	0	1	2	2+1	3
T_0[MeV]	270	240	208	187	178

2.2 Effective coupling strength

In the NJL model, for simplification, a constant effective coupling strength G is used. However, the strength of the interaction should depend on the quark and gluon condensate. When calculating at finite temperature and chemical potential, the coupling strength G may also depend on temperature and/or chemical potential [37–41]. Our recent paper [42] gives a detailed explanation of why we modify the coupling constant. In that paper, the specific heat implementation in the OPE framework has been studied for how to pick up the quark feedback from the gluon propagator. In this way, we introduced a modified coupling strength within the framework of the PNJL model. The coupling strength is replaced by

$$G \longrightarrow G_r = G_1 + G_2 \langle \bar{\psi}\psi \rangle. \tag{14}$$

G_1, G_2 can be fitted with pion properties and the results of lattice QCD [43]. From Eq. (5) we can see that through this replacement G will depend on T and μ. The pion mass m_π and pion decay constant f_π we used to determine G_1 and G_2 are the same as those used in lattice QCD calculations, $m_\pi = 135$ MeV and $f_\pi = 87$ MeV. The parameters we used are listed in Table 4. Physically, the vacuum structure of QCD is non-trivial. With the help of different kinds of vacuum condensates the structure can be characterized. Using the QCD sum rule technique, vacuum condensates are also elementary in the description of strong interaction physics. These condensates will have an impact on the gluons propagating in QCD non-perturbative vacuum [44]. Two-quark condensate is commonly recognized to be the most significant of all the condensates in the description of non-perturbative QCD vacuum, so in this paper we have considered its effect.

Table 4.   Parameter set used in our work.

m(MeV)	Λ(MeV)	G_1(MeV^{-2})	G_2(MeV^{-5})
5.6	587.9	5.359×10^{-6}	4×10^{-14}

To see the difference between our modified PNJL model and the normal one, we have calculated the quark condensate $\bar{\psi}\psi$, Polyakov loop potential ϕ and some QCD thermodynamic quantities as a comparison. The three-momentum cut-off Λ and current quark mass m are the same. Letting the coupling strength G_0 of the original model have the same numerical value as $G = G_1 + G_2 \langle \bar{\psi}\psi \rangle$ at $T = 0$, $\mu = 0$, we get

$$G_0 = G_1 + G_2 \langle \bar{\psi}\psi \rangle |_{T=0, \mu=0} = 6.335 \times 10^{-6} (\text{MeV}^{-2}). \tag{15}$$

We can see that only some quantities have been influenced, with some changed a little. In Fig. 1 and Fig. 2, we have plotted $\langle \bar{\psi}\psi \rangle$ and ϕ for both Potential I and Potential II. It can be seen that the transition temperature of the condensate becomes smaller when we use G_r to replace G at $T_0 = 170$ MeV. This is reasonable because new lattice data show that the critical temperature is smaller than in the previous lattice data, around $T_c = 150 \pm 5$ MeV [35, 43, 45]. The Polyakov loop ϕ is almost the same as in the normal PNJL model. The inflection point of the chiral condensate is almost the same as the confinement-deconfinement transition. The confinement-deconfinement transition happens only a little earlier than the crossover temperature for both Potential I and Potential II.

In quantum field theory, susceptibilities are the linear responses of QCD condensate to various variables [46]. We have calculated the susceptibility of $\langle \bar{\psi}\psi \rangle$ and ϕ to the linear responses of temperature

$$\chi_{\langle \bar{\psi}\psi \rangle} = \frac{\partial \langle \bar{\psi}\psi \rangle}{\partial T}, \qquad \chi_\phi = \frac{\partial \phi}{\partial T}. \tag{16}$$

$\chi_{\langle \bar{\psi}\psi \rangle}$ and χ_ϕ are plotted separately for the two versions of the model in Figs. 3–6. The transition points of the chiral phase transition happen at almost the same T in the two versions of the Polyakov loop potential, as does the susceptibility of the Polyakov loop ϕ. The difference is that Fig. 4 for Potential II has two peaks, a small one and a big one. The two peaks are the transition points of the confinement-deconfinement transition and chiral condensate separately. The transition T of the confinement-deconfinement transition for Potential I is bigger than Potential II. This makes the distance between the transition points of the confinement-deconfinement transition and chiral condensate in the model smaller than for Potential II. Thus when $T_0 = 170$ MeV, the confinement-deconfinement transition happens earlier than the crossover. This is the same as in Ref. [47]. We will interpret this in detail later.
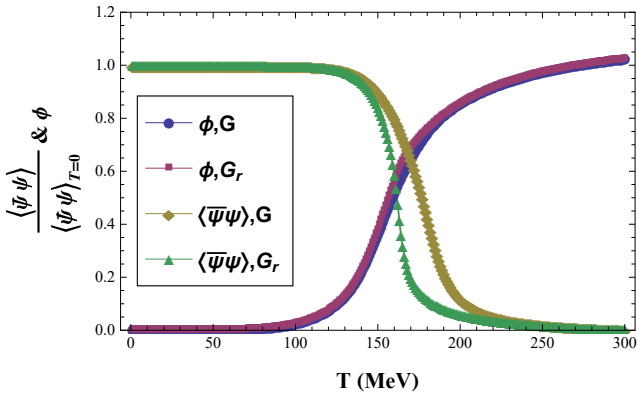
Fig. 1.   (color online) Dependence of the quark condensate and Polyakov loop potential on temperature T for Potential I at $T_0 = 170$ MeV.
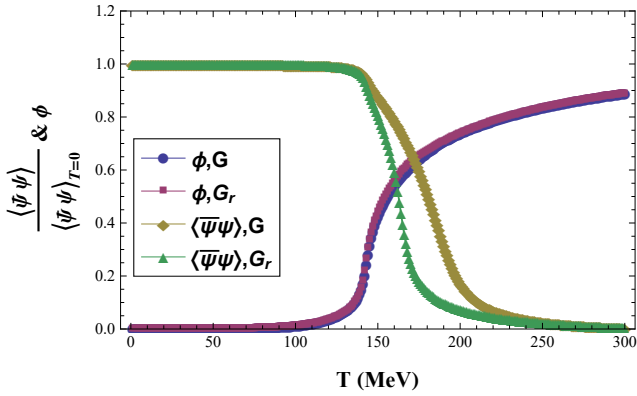

Fig. 2.   (color online) Dependence of the quark condensate and Polyakov loop potential on temperature T for Potential II at $T_0 = 170$ MeV.
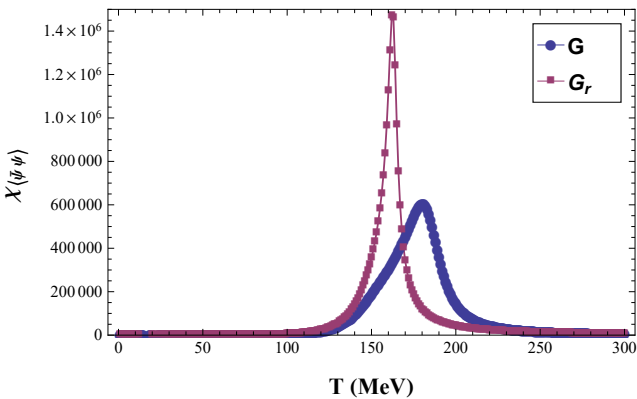

Fig. 3.   (color online) Dependence of the susceptibility $\chi_{\langle \bar{\psi}\psi \rangle}$ on temperature T for Potential I at $T_0 = 170$ MeV.
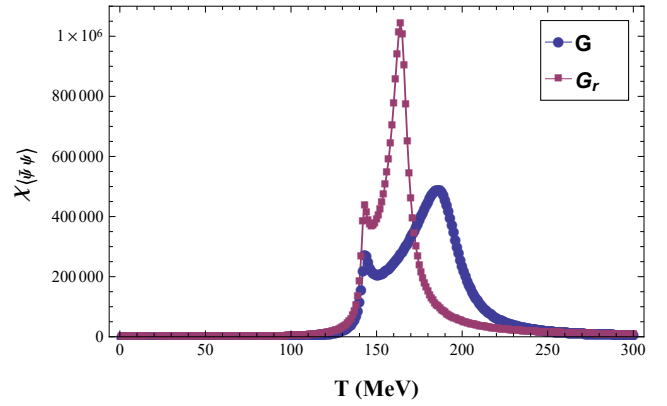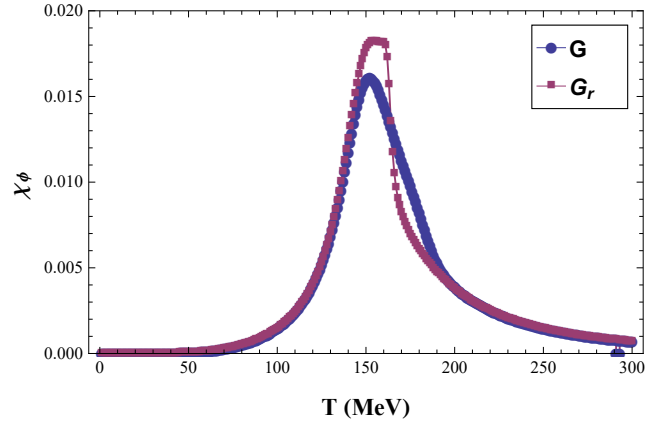

Fig. 4.   (color online) Dependence of the susceptibility $\chi_{\langle \bar{\psi}\psi \rangle}$ on temperature T for Potential II at $T_0 = 170$ MeV.

Fig. 5.   (color online) Dependence of susceptibility χ_ϕ on temperature T for Potential I at $T_0 = 170$ MeV.
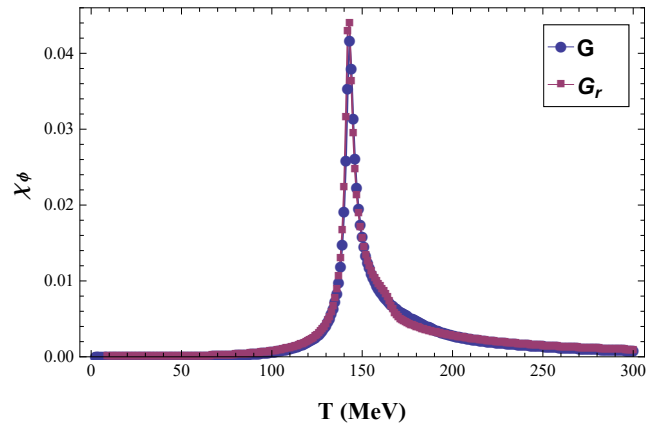
Fig. 6.   (color online) Dependence of susceptibility χ_ϕ on temperature T for Potential II at $T_0 = 170$ MeV.

3   Thermodynamic quantities

We will calculate a couple of thermodynamic quantities and compare the results from the PNJL model and

recent lattice QCD calculations so as to address the effects of the modified Polyakov loop on equilibrium thermodynamics. The bulk thermodynamic observables that are sensitive to transforming from hadronic to quark-gluon degrees of freedom, such as P, ϵ, s, C_V and ν_s, can reflect some aspects of the deconfinement transition. All the messages of the system given by Ω in Eq. (6) are included in the grand canonical potential evaluated at the mean-field extent.

The pressure is

$$P(T) = -\Omega(T), \qquad (17)$$

where $P(0) = 0$ is the vacuum normalization. In the model calculations, pressure is the most important observable and by differentiation we can get other thermodynamic quantities. The trace anomaly $\frac{\Theta^\mu_\mu(T)}{T^4}$ is the quantity easiest to evaluate in lattice QCD. It is in units of the fourth power of T. The trace anomaly is determined by the derivative of $\frac{P(T)}{T^4}$ with T,

$$\frac{\Theta^\mu_\mu(T)}{T^4} = \frac{\Delta}{T^4} = \frac{\epsilon - 3P}{T^4} = \frac{\partial}{\partial T}\left(\frac{P}{T^4}\right), \qquad (18)$$

where ϵ is the energy density. $\frac{\Delta}{T^4}$ is the interaction measure, which is plotted in Fig. 11 and Fig. 12. The maximum value of interaction measure in the modified model is larger than in the normal PNJL model and T is smaller than in the normal PNJL model. The straightforward expectation values are needed in the calculation of the trace anomaly. Integrating over the trace of Θ^μ_μ, we can obtain the pressure,

$$P(T) = P(T_i) + \int_{T_i}^{T} \mathrm{d}T' \frac{1}{T'^5}\Theta^\mu_\mu, \qquad (19)$$

where $P(T_i)$ is the integration constant. For the purpose of making the constant as small as possible, the temperature T_i is adjusted accordingly, and as a result $P(T_i)$ finally drops. T_i is often chosen in the low-temperature area as a random temperature value. In this region P and other thermodynamical quantities are suppressed exponentially by Boltzmann factors related to the lightest hadronic states, i.e. the pions.

In the Stefan-Bolztman (SB) limit, the QCD pressure for $(N_c^2 - 1)$ massless gluons and N_f massless quarks, related to the deconfined phase, is determined at high temperature as [28],

$$\begin{aligned} \frac{P_{\mathrm{SB}}}{T^4} &= \frac{1}{45}\pi^2(N_c^2 - 1) \\ &+ N_c N_f\left(\frac{7\pi^2}{180} + \frac{1}{6}\left(\frac{\mu}{T}\right)^2 + \frac{1}{12\pi^2}\left(\frac{\mu}{T}\right)^4\right), \end{aligned} \qquad (20)$$

where the first term is the gluon contribution. However, in the NJL model, there are no gluons are involved, thus the leading term in the above equation make no contribution. Hence, the NJL model at high temperatures will

give a smaller pressure. The PNJL model will improve this case at high temperature. We have plotted the ratio of pressure in our model and in the ideal gas limit in Fig. 15 and Fig. 16. From these figures we can see that the replacement of the coupling makes little difference. The SB limits are plotted in Fig. 7 and Fig. 8.

With thermodynamic potential Ω we can get the entropy density [6]

$$s = -\left.\frac{\partial\Omega}{\partial T}\right|_V, \qquad (21)$$

and we can get energy density from the relationship

$$\epsilon = -T^2\frac{\partial}{\partial T}\left(\frac{\Omega}{T}\right)\bigg|_V = -T\left(\frac{\partial\Omega}{\partial T}\right)\bigg|_V + \Omega. \qquad (22)$$

We can see from the above two equations that $\epsilon = -P + Ts$. We have also plotted the energy density in Fig. 7 and Fig. 8. At high temperature we hope that P/T^4. For a gas of gluons and N_f quark flavors, ϵ/T^4 will
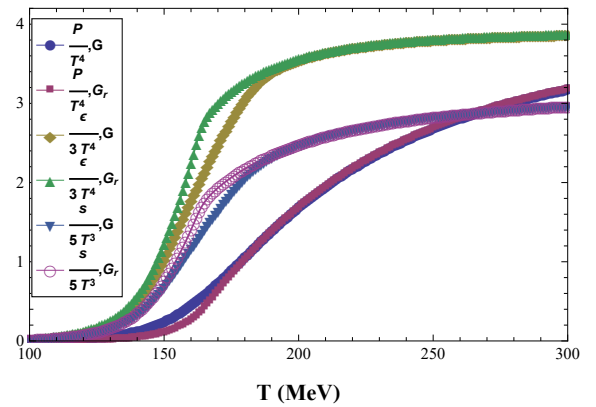
Fig. 7.   (color online) The pressure $\frac{P}{T^4}$, energy density $\frac{\epsilon}{3T^4}$ and entropy density $\frac{s}{5T^3}$ for Potential I at $T_0 = 170$ MeV.
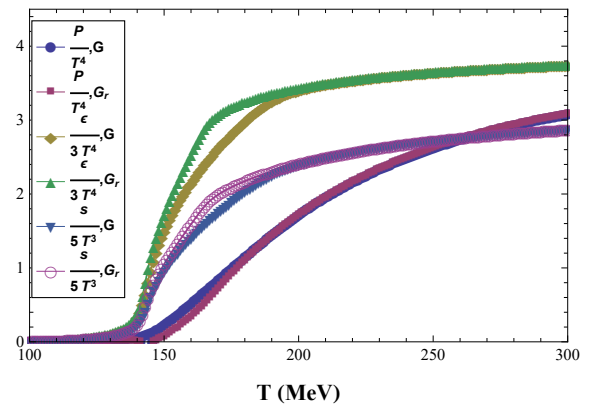
Fig. 8.   (color online) The pressure $\frac{P}{T^4}$, energy density $\frac{\epsilon}{3T^4}$ and entropy density $\frac{s}{5T^3}$ for Potential II at $T_0 = 170$ MeV.
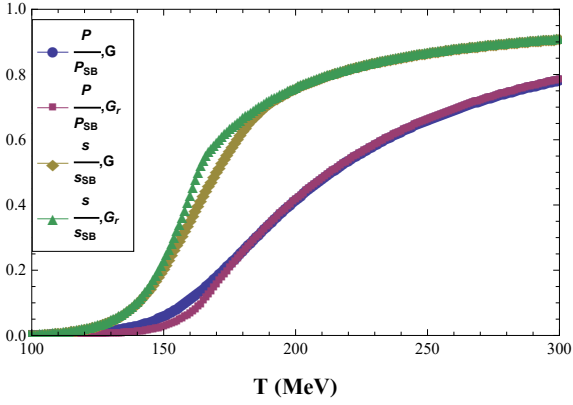
Fig. 9.   (color online) The ratio of pressure (entropy density) in our model and pressure (entropy density) of the ideal gas limit for Potential I at T_0=170 MeV.
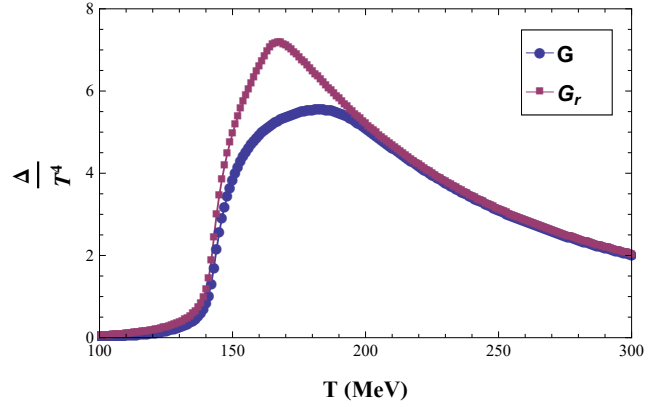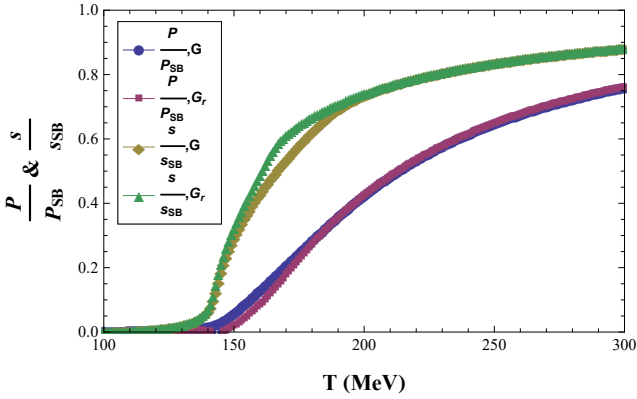

Fig. 10.   (color online) The ratio of pressure (entropy density) in our model and pressure (entropy density) of the ideal gas limit for Potential II at T_0=170 MeV.
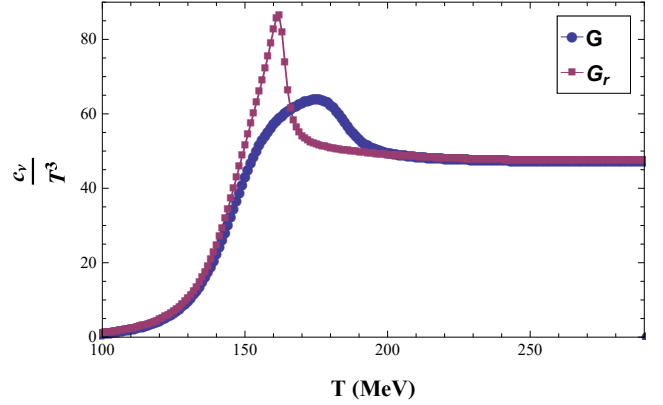

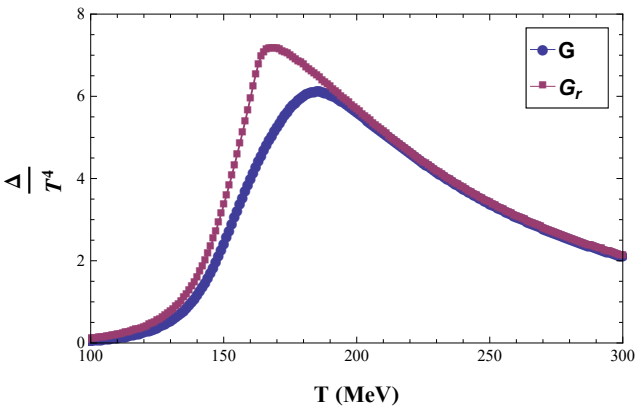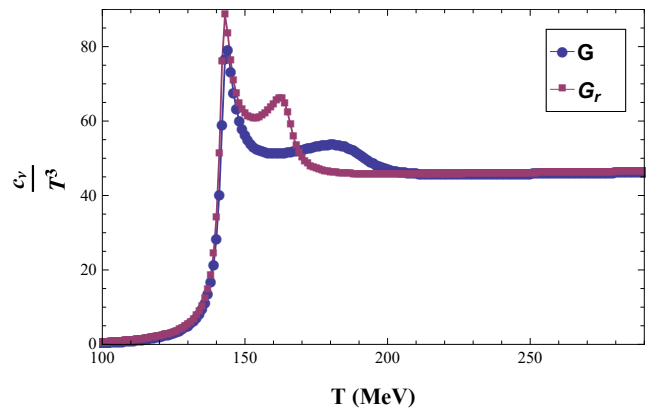Fig. 11.   (color online) The interaction measure for Potential I at T_0=170 MeV.

Fig. 12.   (color online) The interaction measure for Potential II at T_0=170 MeV.

Fig. 13.   (color online) Specific heat for Potential I at T_0=170 MeV.

Fig. 14.   (color online) Specific heat for Potential II at T_0=170 MeV.
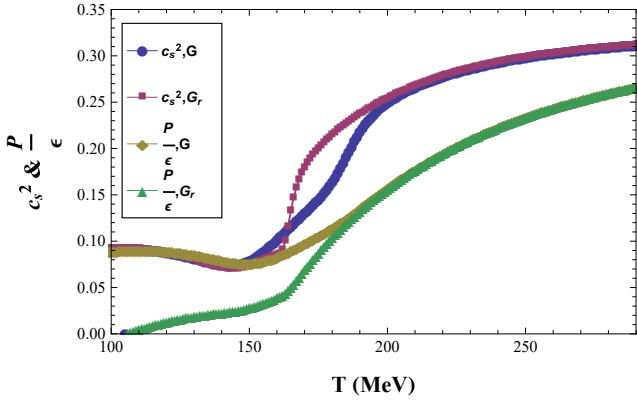
Fig. 15.   (color online) Speed of sound ν_s^2 and the ratio of pressure and energy density $\frac{P}{\epsilon}$ for Potential I at $T_0 = 170$ MeV.
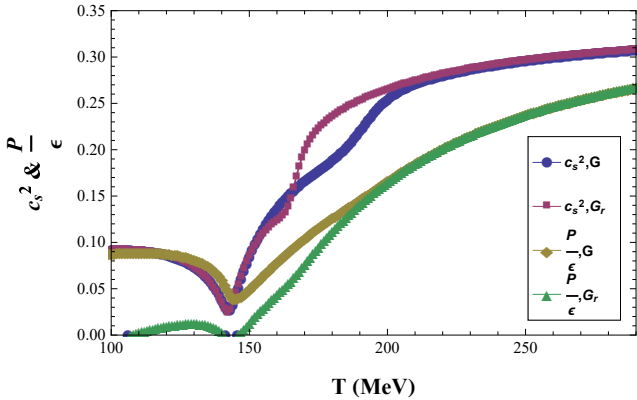

Fig. 16.   (color online) Speed of sound ν_s^2 and the ratio of pressure and energy density $\frac{P}{\epsilon}$ for Potential II at $T_0 = 170$ MeV.

asymptotically approach the free gas limit,

$$\frac{\epsilon_{\mathrm{SB}}}{T^4} = \frac{3P_{\mathrm{SB}}}{T^4} = \left(16 + \frac{21}{2}N_f\right)\frac{\pi^2}{30}. \quad (23)$$

When $N_f = 2$, we can see that $\epsilon_{\mathrm{SB}} = 12.160$ and $P_{\mathrm{SB}} = 4.053$. From Fig. 9 and Fig. 10 we can see that the two ratios all reach 1 with increasing temperature. Potential II seems smaller than Potential I.

The specific heat is obtained from the partial derivative of ϵ with T at definite volume:

$$C_V = \frac{\partial \epsilon}{\partial T}\bigg|_V = -\frac{\partial^2 \Omega}{\partial T^2}\bigg|_V. \quad (24)$$

For a continuous phase transition, the divergence in C_V depends on universality class [7]. In the case of $Z(2)$ universality class one expects a divergence in C_V, which is related to the event-by-event temperature fluctuations, and mean transverse momentum fluctuations in heavy-ion reactions. These fluctuations will be a divergence near the CEP. The specific heat is plotted in Fig. 13 and Fig. 14. We can see that for Potential I the specific heat has only one peak, while for Potential II it has two peaks.

We can see similar behavior in the next section and try to explain it there.

The square of the velocity of sound at finite entropy (S) is determined by

$$\nu_s^2 = \frac{\partial P}{\partial \epsilon}\bigg|_S = \frac{\partial P}{\partial T}\bigg|_V \bigg/ \frac{\partial \epsilon}{\partial T}\bigg|_V = \frac{\partial \Omega}{\partial T}\bigg|_V \bigg/ T\frac{\partial^2 \Omega}{\partial T^2}\bigg|_V. \quad (25)$$

From the above equation we can see that $\nu_s^2 = \frac{s}{C_V}$. Since the denominator is C_V, a divergence in C_V means that the speed of sound becomes zero at the CEP. Therefore, a prominent dip near the chiral and deconfinement transition points to the speed of sound. In all the models, including the NJL model, at high temperature, ν_s^2 approaches the ideals gas value $1/3$ and can be approximated to the ratio P/ϵ. Furthermore, the numerical value of P/ϵ is in accordance with that of ν_s^2 for low temperatures [27]. In the high temperature limit the ratio P/ϵ can approach it. For comparison, we have plotted ν_s^2 and P/ϵ in the same diagram in Fig. 15 and Fig. 16 for Potential I and Potential II respectively.

The conformal measure $\mathcal{C}$ is defined as

$$\mathcal{C} = \frac{\Delta}{\epsilon} = \frac{\epsilon - 3P}{\epsilon} \simeq 1 - 3\nu_s^2. \quad (26)$$

Thus, near the phase transition or crossover a minimum of the velocity of sound will result in a maximum in conformal measure $\mathcal{C}$. When approaching the asymptotic temperature where the ideal gas value $1/3$, the conformal measure should approach to the conformal measure limit $\mathcal{C} = 0$.

4 T_0 dependence

We have changed T_0 to see how $\langle\bar{\psi}\psi\rangle$, ϕ, $\mathcal{C}$, C_V and ν_s^2 changes with it in the normal PNJL model. The lattice data for the condensate are taken from Ref. [43]. In Figs. 17–30, we have plotted the QCD thermodynamic quantities in both models. On one hand, we can see that when T_0 becomes smaller, the transition temperature also becomes smaller, and the changing of condensate becomes closer to that of lattice data. The two models give us different results; for example, almost all values for Potential II are smaller than for Potential I. However, the specific heat for Potential II is larger than for Potential I and the peak happens earlier. Furthermore, the susceptibility of condensate and specific heat have two peaks for Potential II when temperature $T_0 = 100$ MeV, $T_0 = 150$ MeV, $T_0 = 200$ MeV, and the locations of the two peaks are exactly the maximum values of condensate and Polyakov loop susceptibility respectively. When T_0 becomes bigger, the two peaks become closer, and finally become one peak when $T_0 = 270$ MeV. In fact, as well as condensate susceptibility and specific heat for Potential II being affected, we can see from Figs. 27–30 that for ν_s^2, P/ϵ and ϵ, when T_0 is small, after the minimum value,

Fig. 17.   (color online) T_0 dependence of the quark condensate for Potential I.
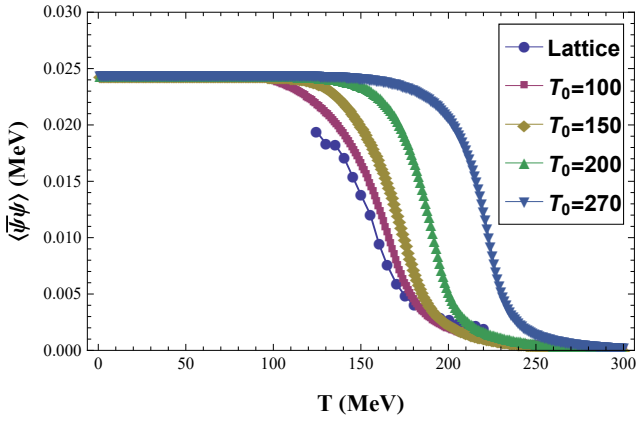

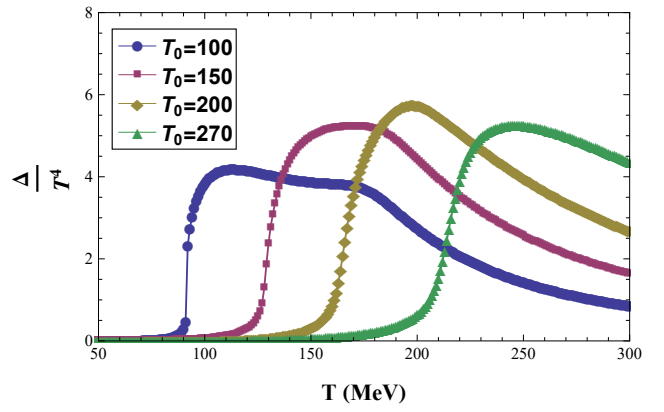Fig. 18.   (color online) T_0 dependence of the quark condensate for Potential II.

Fig. 19.   (color online) T_0 dependence of the interaction measure for Potential I.
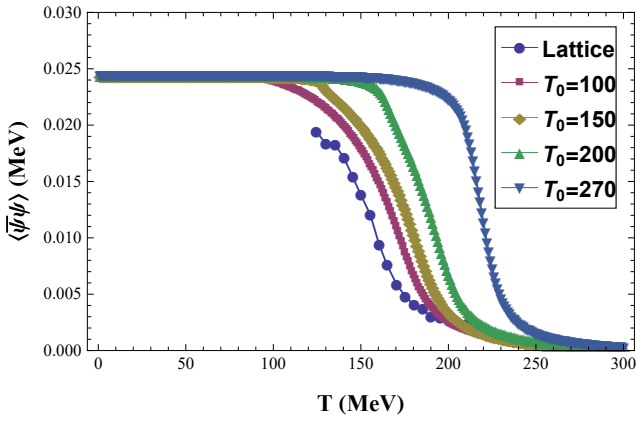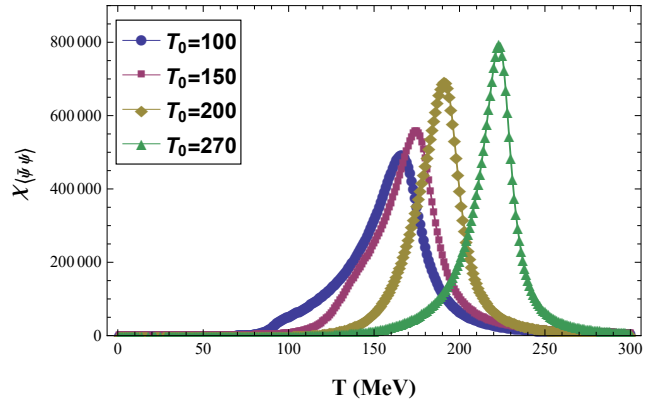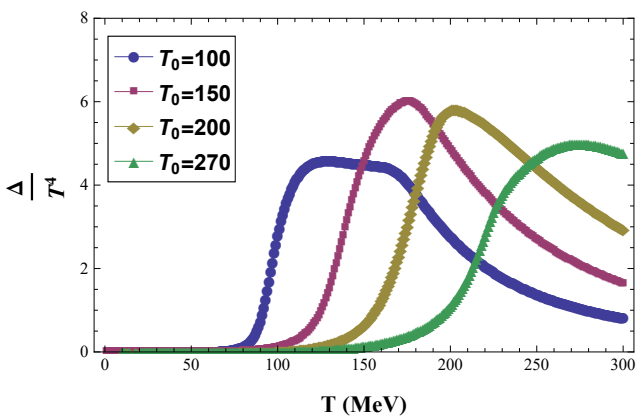

Fig. 20.   (color online) T_0 dependence of the interaction measure for Potential II.

Fig. 21.   (color online) T_0 dependence of the susceptibility $\chi_{\langle\bar\psi\psi\rangle}$ for Potential I.
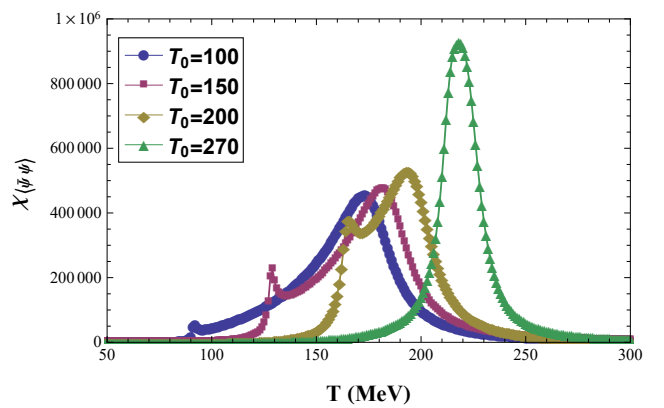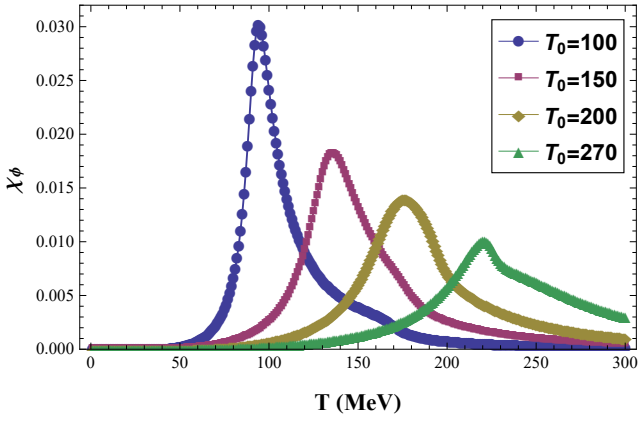

Fig. 22.   (color online) T_0 dependence of the susceptibility $\chi_{\langle\bar\psi\psi\rangle}$ for Potential II.

Fig. 23.   (color online) T_0 dependence of the susceptibility χ_ϕ for Potential I.
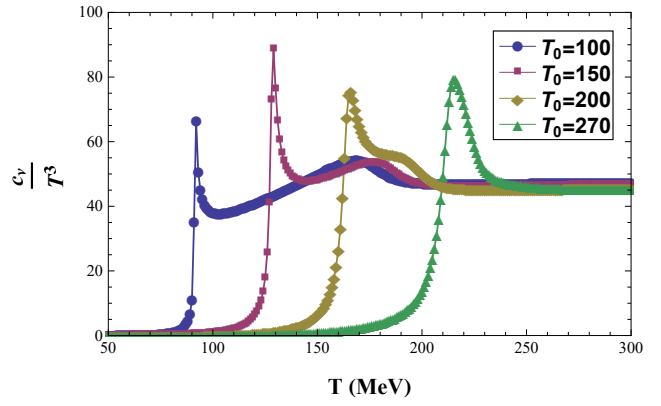

Fig. 24.   (color online) T_0 dependence of the susceptibility χ_ϕ for Potential II.

Fig. 25.   (color online) T_0 dependence of the specific heat for Potential I.

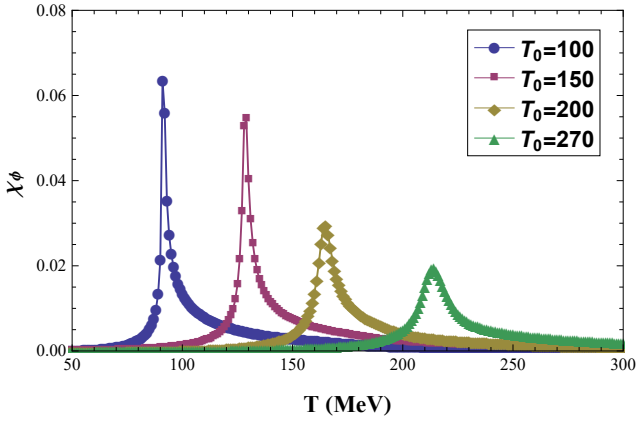Fig. 26.   (color online) T_0 dependence of the specific heat for Potential II.
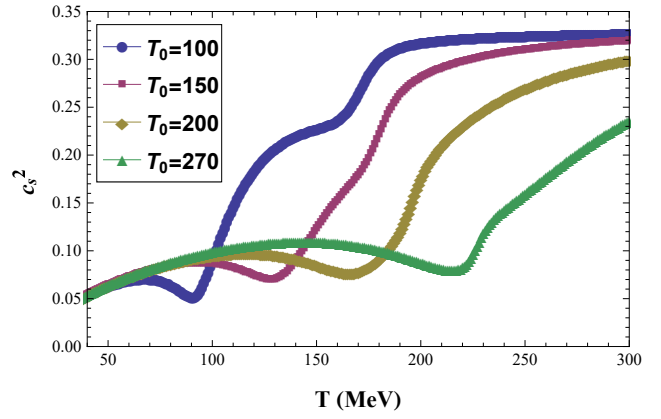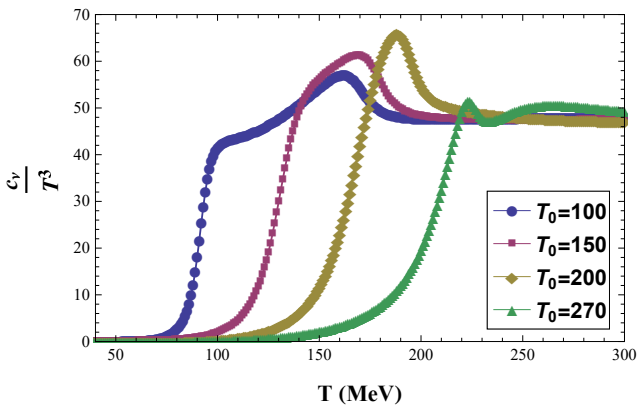

Fig. 27.   (color online) T_0 dependence of the speed of sound for Potential I.
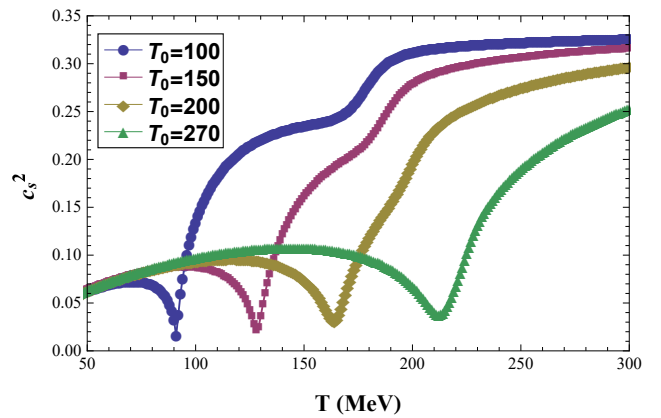

Fig. 28.   (color online) T_0 dependence of the speed of sound for Potential II.
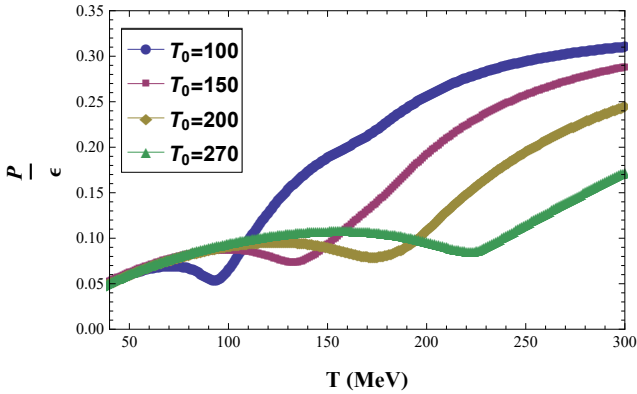
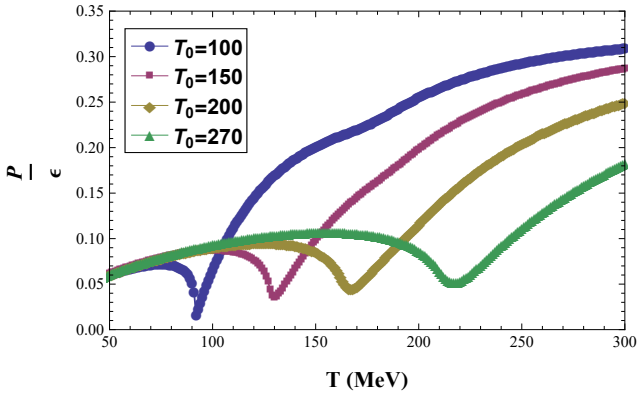Fig. 29.   (color online) T_0 dependence of the ratio of pressure and energy density for Potential I.

Fig. 30.   (color online) T_0 dependence of the ratio of pressure and energy density for Potential II.

the lines seem not to be smooth and have a tendency to drop a little, although it is not too obvious. When T_0 becomes bigger, the lines become more and more smooth after the minimum value. The specific heat for Potential I also has this tendency. However, the transition point of confinement-deconfinement changes more quickly than the transition point of the crossover, and when T_0 is small, it seems that the confinement-deconfinement transition happens earlier than crossover. With increasing T_0, the two transition points become closer. So, the common belief that the inflection points of chiral condensate and confinement-deconfinement transitions happen at the same T in the PNJL model may just be a coincidence. With a different value of T_0, they will no longer happen at the same temperature.

We have tried to explain why the specific heat has two peaks. If the crossover and confinement-deconfinement transitions do not happen at the same T, the specific heat may have a peak at both transition points. From this point, if lattice QCD can calculate C_V or ν_s^2 when the chiral transition happens around $T_c = 150$ MeV, we can compare our data with it. In this case, if the lattice QCD data have two peaks, it may demonstrate

that the crossover and confinement-deconfinement transitions happen at different T. If the lattice QCD data show only one peak, it may prove that the crossover and confinement-deconfinement transitions happen at the same T.

5   Summary and conclusions

The chiral phase transition and confinement-deconfinement phase transition are two of the most basic phase transitions of strongly interacting matter. However, there is no final consensus in the lattice community on the coincidence of the chiral phase transition and confinement-deconfinement transition, although it is widely believed that the two transitions do coincide. Therefore, the main purpose of our paper is to study the relationship of chiral phase transition and confinement-deconfinement. In this paper, we have studied the modified PNJL model with $G_r = G_1 + G_2 \langle \bar{\psi}\psi \rangle$ when $T_0 = 170$ MeV, in two different forms of Polyakov loop potential. Comparing the results of the two potentials, we find that crossover and confinement-deconfinement transitions happen at different places. The transition points of the chiral condensate and confinement-deconfinement transitions in different models are at almost the same temperature. The specific heat has different behaviors; for $\mathcal{U}_{\log}$ it seems to have two peaks in both modified and unmodified models, but when the potential becomes $\mathcal{U}_{\text{poly}}$ it seems to be only one peak. The inflection point of the chiral condensate and confinement-deconfinement for Potential II is nearer than Potential I. Due to the lack of lattice data on thermodynamic quantities of two-flavor QCD, it is difficult to conclude which of the Polyakov loop potentials is better compared with lattice data. However, when extending our model to $n_f = 2+1$ flavor QCD, there will be more lattice data, such as Refs. [48–51], which have given entropy density and speed of sound. Using the recent stable and continuum extrapolated lattice QCD, Ref. [50] shows the specific heat does not have a peak for $n_f = 2+1$ flavor QCD. Reference [43] shows that the infection point of light quark chiral condensate is around 150 MeV. We can extend our model to $n_f = 2+1$ flavors for our future work, and compare with the corresponding lattice data.

We have also calculated several important thermodynamic quantities like interaction measure, energy density, entropy density, specific heat and speed of sound. Comparing these with the ideal values, we find that they all fit well. To see how these quantities depend on T_0, we have chosen four different values of T_0. From these diagrams we can see that when T_0 becomes smaller, the inflection points of chiral condensate and confinement-deconfinement become smaller, but the confinement-deconfinement transition changes quicker than crossover. So when T_0 become small enough, the confinement-

deconfinement transition happens earlier than crossover. For Potential II, the two peaks become one with increasing T_0, which means that the inflection points of chiral condensate and confinement-deconfinement become closer. The belief that confinement-deconfinement transition and crossover happen at the same point in the PNJL model may be an accident. When T_0 changes, these transitions may happen at different temperatures, and in fact T_0 is not always 270 MeV because it will change with quark flavor. If lattice QCD or other QCD experiments can calculate that the inflection point of chiral condensate happens around 150 MeV, and specific heat has two peaks, it may be a demonstration that

confinement-deconfinement transition and crossover happen at different temperatures. If specific heat has one peak, it may verify that the two transitions happen at the same temperature. It is straightforward to extend the PNJL model from finite temperature to finite temperature and finite chemical potential [18]. Generalizing to finite temperature and finite chemical potential is also very meaningful, because we can not only study the phase diagram of strongly interacting matter, but also obtain the equation of state of strongly interacting matter, which is very important to study the structures and properties of neutron stars.

References

1 K. Fukushima, Phys. Rev. D, **77**: 114028 (2008)
2 H. Abuki, R. Anglani, R. Gatto, G. Nardulli, and M. Ruggieri, Phys. Rev. D, **78**: 034034 (2008)
3 S. P. Klevansky, Rev. Mod. Phys., **64**: 649 (1992)
4 M. Buballa, Phys. Rep., **407**: 205 (2005)
5 M. Ciminale, R. Gatto, N. D. Ippolito, G. Nardulli, and M. Ruggieri, Phys. Rev. D, **77**: 054023 (2008)
6 S. K. Ghosh, T. K. Mukherjee, M. G. Mustafa, and R. Ray, Phys. Rev. D, **73**: 114007 (2006)
7 H.-T. Ding, F. Karsch, and S. Mukherjee, Int. J. Mod. Phys. E, **24**: 1530007 (2015), arXiv:1504.05274 [hep-lat]
8 H. Hansen, W. M. Alberico, A. Beraudo, A. Molinari, M. Nardi, and C. Ratti, Phys. Rev. D, **75**: 065004 (2007)
9 Y. Sakai, K. Kashiwa, H. Kouno, and M. Yahiro, Phys. Rev. D, **77**: 051901 (2008)
10 P. Costa, M. C. Ruivo, C. A. de Sousa, H. Hansen, and W. M. Alberico, Phys. Rev. D, **79**: 116003 (2009)
11 C. Ratti, S. Roessner, M. A. Thaler, and W. Weise, Proceedings, Workshop for Young Scientists on the Physics of Ultrarelativistic Nucleus-Nucleus Collisions (Hot Quarks 2006): Villasimius, Italy, May 15-20, 2006, Eur. Phys. J. C., **49**: 213 (2007), arXiv:hep-ph/0609218 [hep-ph]
12 Z. Zhang and Y.-X. Liu, Phys. Rev. C, **75**: 064910 (2007), arXiv:hep-ph/0610221 [hep-ph]
13 K. Kashiwa, H. Kouno, and M. Yahiro, Phys. Rev. D, **80**: 117901 (2009), arXiv:0908.1213 [hep-ph]
14 G. Hellstern, R. Alkofer, and H. Reinhardt, Nucl. Phys. A, **625**: 697 (1997), arXiv:hep-ph/9706551 [hep–ph]
15 T. Z. Nakano, K. Miura, and A. Ohnishi, Phys. Rev. D, **83**: 016014 (2011), arXiv:1009.1518 [hep-lat]
16 Y. Sakai, T. Sasaki, H. Kouno, and M. Yahiro, J. Phys. G, **39**: 035004 (2012), arXiv:1104.2394 [hep-ph]
17 K.-I. Kondo, Phys. Rev. D, **82**: 065024 (2010), arXiv:1005.0314 [hep-th]
18 Z.-F. Cui, I. C. Cloët, Y. Lu, C. D. Roberts, S. M. Schmidt, S.-S. Xu, and H.-S. Zong, Phys. Rev. D, **94**: 071503 (2016), arXiv:1604.08454 [nucl-th]
19 B. B. Back et al, Nucl. Phys. A, **757**: 28 (2005), arXiv:nucl-ex/0410022 [nucl-ex]
20 J. Adams et al (STAR), Nucl. Phys. A, **757**: 102 (2005), arXiv:nucl-ex/0501009 [nucl-ex]
21 K. Adcox et al, Nucl. Phys. A, **757**: 184 (2005)
22 A. Bazavov et al, Phys. Rev. D, **80**: 014504 (2009), arXiv:0903.4379 [hep-lat]
23 B. Mohanty and J.-e. Alam, Phys. Rev. C, **68**: 064903 (2003)
24 C. Bernard et al, Phys. Rev. D, **75**: 094505 (2007), arXiv:hep-lat/0611031 [hep-lat]
25 M. Cheng et al, Phys. Rev. D, **77**: 014511 (2008), arXiv:0710.0354 [hep-lat]
26 A. Polyakov, Phys. Lett. B, **72**: 477 (1978)
27 B.-J. Schaefer, M. Wagner, and J. Wambach, Phys. Rev. D, **81**: 074013 (2010)
28 C. Ratti, M. A. Thaler, and W. Weise, Phys. Rev. D, **73**: 014019 (2006)
29 S. Rößner, C. Ratti, and W. Weise, Phys. Rev. D, **75**: 034007 (2007)
30 R. D. Pisarski, Phys. Rev. D, **62**: 111501 (2000)
31 A. Dumitru and R. D. Pisarski, Phys. Lett. B, **525**: 95 (2002), arXiv:hep-ph/0106176 [hep-ph]
32 K. Fukushima, Phys. Lett. B, **591**: 277 (2004), arXiv:hep-ph/0310121 [hep-ph]
33 C. Ratti, S. Roessner, and W. Weise, Phys. Lett. B, **649**: 57 (2007), arXiv:hep-ph/0701091 [hep-ph]
34 C. Ratti and W. Weise, Phys. Rev. D, **70**: 054013 (2004)
35 J. Braun and H. Gies, JHEP, **2006**: 024 (2006)
36 B.-J. Schaefer, J. M. Pawlowski, and J. Wambach, Phys. Rev. D, **76**: 074023 (2007)
37 H.-S. Zong, W.-M. Sun, J.-L. Ping, F. Wang et al, Chin. Phys. Lett., **22**: 3036 (2005)
38 Y. Jiang, H. Gong, W.-M. Sun, and H.-S. Zong, Phys. Rev. D, **85**: 034031 (2012)
39 Z.-F. Cui, C. Shi, Y.-H. Xia, Y. Jiang, and H.-S. Zong, Eur. Phys. J. C, **73**: 2612 (2013)
40 Z.-F. Cui, C. Shi, W.-M. Sun, Y.-L. Wang, and H.-S. Zong, Eur. Phys. J. C., **74**: 2782 (2014)
41 C. Shi, Y.-L. Du, S.-S. Xu, X.-J. Liu, and H.-S. Zong, Phys. Rev. D, **93**: 036006 (2016), arXiv:1602.00062 [hep-ph]
42 C.-M. Li, J.-L. Zhang, Y. Yan, Y.-F. Huang, and H.-S. Zong, Phys. Rev. D, **97**: 103013 (2018), arXiv:1804.10785 [nucl-th]
43 S. Borsányi, Z. Fodor, C. Hoelbling, S. D. Katz, S. Krieg, C. Ratti, and K. K. Szabó, JHEP, **2010**: 73 (2010)
44 T. G. Steele, Z. Phys. C-Particles and Fields, **42**: 499 (1989)
45 Y. Aoki, S. Borsányi, S. Drr, Z. Fodor, S. D. Katz, S. Krieg, and K. Szabó, JHEP **2009**: 88 (2009)
46 Z.-F. Cui, F.-Y. Hou, Y.-M. Shi, Y.-L. Wang, and H.-S. Zong, Annals Phys., **358**: 172 (2015), arXiv:1505.00310[hep-ph]
47 I. General, D. G. Dumm, and N. Scoccola, Phys. Lett. B, **506**: 267 (2001)
48 S. Borsanyi, Proceedings, *23rd International Conference on Ultrarelativistic Nucleus-Nucleus Collisions: Quark Matter 2012 (QM 2012)*: Washington, DC, USA, August 13-18, 2012, Nucl. Phys. A904-905, 270c (2013), arXiv:1210.6901 [hep-lat]
49 S. Borsanyi, G. Endrodi, Z. Fodor, A. Jakovac, S. D. Katz, S. Krieg, C. Ratti, and K. K. Szabo, JHEP, **11**: 077 (2010), arXiv:1007.2580 [hep-lat]
50 A. Bazavov et al (HotQCD), Phys. Rev. D, **90**: 094503 (2014), arXiv:1407.6387 [hep-lat]
51 S. Borsanyi, Z. Fodor, C. Hoelbling, S. D. Katz, S. Krieg, and K. K. Szabo, Phys. Lett. B, **730**: 99 (2014), arXiv:1309.5258 [hep-lat]